

Cassini State Capture

Yubo Su¹, Dong Lai¹

¹ *Cornell Center for Astrophysics and Planetary Science, Department of Astronomy, Cornell University, Ithaca, NY 14853, USA*

Accepted XXX. Received YYY; in original form ZZZ

ABSTRACT

Abstract

Key words: planet–star interactions

1 INTRODUCTION

Introduction, test citation (Henrard 1982).

2 CASSINI STATES

Denote \hat{s} spin of planet, \hat{l} angular momentum of planet, and \hat{l}_p angular momentum of perturber. The Cassini state Hamiltonian in the frame corotating with \hat{l}_p about \hat{l} is:

$$H = -\frac{\alpha}{2} (\hat{s} \cdot \hat{l})^2 - g (\hat{s} \cdot \hat{l}_p). \quad (1)$$

$\alpha > 0, g < 0$ depend on the particular dynamics of the system. Frequently, parameter

$$\eta \equiv \frac{|g|}{\alpha} \quad (2)$$

is defined; we refrain from doing so immediately.

Choose $\hat{l} = \hat{z}$ and $\hat{l}_p = \cos I \hat{z} + \sin I \hat{x}$. Furthermore, choose standard convention where $\phi = 0$ corresponds to \hat{l}_p, \hat{s} lying on opposite sides of \hat{l} . This allows us to evaluate Hamiltonian

$$H = -\frac{\alpha}{2} \cos^2 \theta + |g| (\cos \theta \cos I - \sin I \sin \theta \cos \phi) \quad (3)$$

Here, $\mu \equiv \cos \theta, \phi$ are canonically conjugate.

2.1 Equilibria

The evolution of \hat{s} in this corotating frame is governed by:

$$\frac{d\hat{s}}{dt} = \alpha (\hat{s} \cdot \hat{l}) (\hat{s} \times \hat{l}) - |g| (\hat{s} \times \hat{l}_p). \quad (4)$$

Spin states satisfying $\frac{d\hat{s}}{dt} = 0$ are referred to as *Cassini States* (CS). When $\eta < \eta_c$, there are four CSs, and when $\eta > \eta_c$ there are only two; η_c is

$$\eta_c \equiv \left(\sin^{2/3} I + \cos^{2/3} I \right)^{3/2}. \quad (5)$$

Using the standard numbering given in Figure 1, CSs 1, 2, 3 are stable while CS4 is unstable.

2.2 Separatrix

In the four-CS regime, one of the CSs is a saddle point, conventionally denoted Cassini State 4 (CS4). On the cylindrical phase space parameterized by (μ, ϕ) , all trajectories are periodic with finite period except two critical (or heteroclinic) trajectories. These are asymptotic in the past and future to CS4. Together, these two heteroclinic are referred to as the *separatrix* and divide phase space into three zones.

The area enclosed by the separatrix is known exactly in literature (Henrard & Murigande 1987), but a serviceable approximation for small η can be derived as follows. Call H_{sep} the value of H along the separatrix (also the value of H at CS4), then the separatrix is defined implicitly by solutions to $H(\mu_{sep}(\phi), \phi) = H_{sep}$. This may be evaluated and we obtain

$$\mu_{sep}(\phi) \approx \pm \sqrt{2\eta \sin I (1 - \cos \phi)} + \eta \cos I + O(\eta^{3/2}). \quad (6)$$

The enclosed area between the two solutions can be obtained via explicit integration. It can be expressed as a fraction of the total phase space area:

$$\frac{A_{sep}}{4\pi} \approx \frac{4\sqrt{\eta \sin I}}{\pi} + O(\eta^{3/2}). \quad (7)$$

Contours of equal H , CSs and the separatrix are plotted in Figure 1.

3 SEPARATRIX CROSSING: THEORY

In an exactly Hamiltonian system, H is a conserved quantity and trajectories in phase space coincide with level curves of H . If a system is only slightly non-Hamiltonian, trajectories will generally cross level curves. Of particular interest is the behavior of trajectories near the separatrix (also a level curve), as it frequently governs the dynamics of resonance capture (CITE MMR, Cassini, others). The intersection of system trajectories with the separatrix is referred to as *separatrix crossing*.

In previous work by Henrard (1982), separatrix crossing was studied for systems that are Hamiltonian save for an adiabatically-varying parameter. In related work surveyed by Guckenheimer & Holmes (1983), the impact of small perturbations to the equations of motion of a Hamiltonian system are studied (referred to as *saddle connection bifurcations*). However, in some astrophysical systems

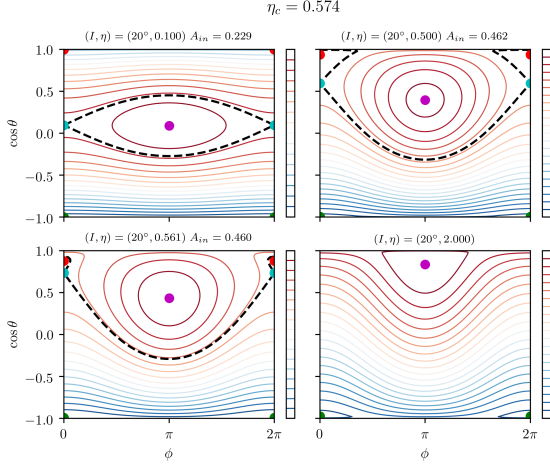


Figure 1. Contours of equal H , given by Equation 3, at different values of $\eta \equiv \frac{g}{\alpha}$. Labeled are CS1 (red), CS2 (purple), CS3 (green) and CS4 (cyan). The thick black dashed line is the separatrix (which disappears for $\eta > \eta_c$). Finally, the fractional area enclosed by the separatrix is noted in the plot subtitles, in good agreement with Equation 7.

of interest, leading-order perturbations to a Hamiltonian system contribute in both of the above ways. Such systems resist characterization via either existing technique. We suggest a possible generalization unifying the above techniques. [Probably eventually move this paragraph to the introduction]

3.1 Derivation

Consider our Hamiltonian described in Equation 3 as a unperturbed Hamiltonian $H^{(0)}(\mu, \phi; \eta)$ where η is to be varied adiabatically. As η varies, the location of the separatrix also changes. We follow Henrard (1982) by defining

$$h(\mu, \phi; \eta) \equiv H^{(0)}(\mu, \phi; \eta) - H_{sep}(\eta). \quad (8)$$

The significance of h is that it always vanishes along the separatrix. Note that h corresponds to K in Henrard (1982), though in our problem $H^{(0)} > H_{sep}$ corresponds to the *interior* of the separatrix. The evolution of h over time then determines whether and when a trajectory experiences separatrix crossing. Denoting time derivatives with dots, we write

$$\begin{aligned} \frac{dh}{dt} &= \frac{dH^{(0)}}{dt} - \frac{\partial H_{sep}}{\partial \eta} \dot{\eta}, \\ &= \left[\frac{\partial H^{(0)}}{\partial \mu} \dot{\mu} + \frac{\partial H^{(0)}}{\partial \phi} \dot{\phi} + \frac{\partial H^{(0)}}{\partial \eta} \dot{\eta} \right] - \frac{\partial H_{sep}}{\partial \eta} \dot{\eta}, \\ &= \left[\frac{\partial H^{(0)}}{\partial \mu} \dot{\mu} + \frac{\partial H^{(0)}}{\partial \phi} \dot{\phi} + \frac{\partial H^{(0)}}{\partial \eta} \dot{\eta} \right] - \frac{\partial H_{sep}}{\partial \eta} \dot{\eta}, \\ &= \left[\dot{\phi}^{(0)} \dot{\mu}^{(1)} - \dot{\mu}^{(0)} \dot{\phi}^{(1)} + \frac{\partial H^{(0)}}{\partial \eta} \dot{\eta} \right] - \frac{\partial H_{sep}}{\partial \eta} \dot{\eta}. \end{aligned} \quad (9)$$

We've notated $\dot{\phi}^{(0)} \equiv \frac{\partial H^{(0)}}{\partial \mu}$ and $\dot{\phi}^{(1)} = \dot{\phi} - \dot{\phi}^{(0)}$ and similarly for μ . The scenario studied in Henrard (1982) corresponds to $\dot{\mu}^{(1)} = \dot{\phi}^{(1)} = 0$ while that in Guckenheimer & Holmes (1983) sets $\dot{\eta} = 0$.

In the neighborhood of C_{\pm} , the $\frac{dh}{dt}$ can be approximated by its value on C_{\pm} . This is the *guiding orbit* approximation; its accuracy is proven in Henrard (1982) for their specific application, while we

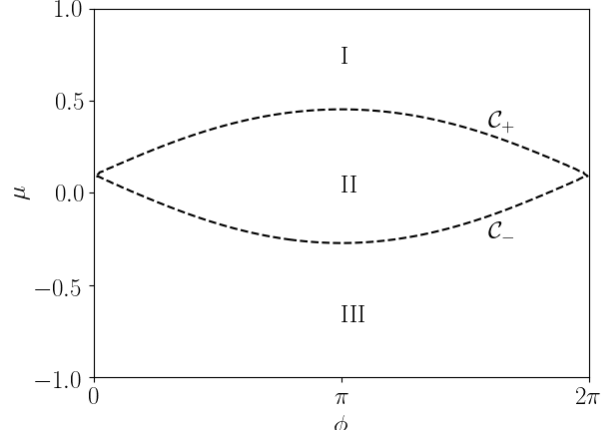


Figure 2. Nomenclature of the two legs of the separatrix C_{\pm} and three zones of the domain. For both C_{\pm} , we will take the positive direction to be anti-clockwise.

will take it on good faith in ours. Denote then

$$\Delta_{\pm} \equiv \int_{C_{\pm}} \frac{dh}{dt} dt. \quad (10)$$

These approximate Δh for trajectories near C_{\pm} over one orbit. They are identical to the B_i defined in Henrard (1982).

3.2 Zone I/III Initial Conditions

For concreteness, we consider a specific example first. We assign labels to our phase space as shown in Figure 2. Consider a trajectory that begins in zone III, which is circulating with $\dot{\phi} > 0$ and has $h < 0$, and consider if $\frac{dh}{dt} > 0$ in all of zone III, such that the trajectory eventually experiences separatrix crossing at C_- . The following sequence of events unfolds:

(i) At the beginning ($\phi = 0$) of its separatrix-crossing orbit, $h_i \equiv h(\mu, \phi = 0; \eta) \in (\Delta_-, 0)$. Note that $h_i < 0$ to still be in zone III at the start of the orbit, while $h_i > \Delta_-$ to be separatrix crossing during the final orbit.

(ii) After traversing the length of C_- , the value of h is now $h_i + \Delta_- > 0$ (recall $\Delta_- > 0$), and so the trajectory has entered zone II. Since zone II hosts only librating solutions, the trajectory will then “turn around” and track C_+ from inside zone II.

(iii) At the end of following C_+ , h now takes value $h_f \equiv h_i + \Delta_- + \Delta_+$. There are now two possibilities:

(iii-a) If $h_f > 0$, the trajectory remains inside zone II accrues further multiples of $\Delta_- + \Delta_+ = h_f - h_i > 0$. Thus, the trajectory must securely enter zone II. This outcome commonly corresponds to *resonance capture*, a transition into zone II.

(iii-b) If $h_f < 0$, the trajectory exits zone II and enters zone I. Since $\Delta_+ = h_f - h_i - \Delta_- < 0$ (as $h_f < 0$, $h_i + \Delta_- > 0$), the trajectory will continue circulation in zone I and accrue further multiples of Δ_+ , securely entering zone I. This corresponds to a zone III-zone I transition, *escape*.

Thus, the result of separatrix crossing depends on the sign of $h_i + \Delta_- + \Delta_+$ where Δ_{\pm} are given by Equation 10 and $h_i \in [-\Delta_-, 0]$. The result of this analysis reproduces the conclusion of Henrard (1982):

- If $\Delta_+ < -\Delta_-$, then $h_f < 0$ necessarily, secure escape ensues.

- If $\Delta_+ > 0$, then $h_f > 0$ necessarily, and secure capture ensues.
- If $\Delta_+ + \Delta_- \in [0, \Delta_-]$, then it is clear that the sign of h_f depends on the precise value of h_i . Generally, Δ_- can be assumed to be small as perturbations are weak, and so Δ_- is usually much smaller than the range of h of interest. Thus, h_i can be treated as uniformly distributed on interval $[-\Delta_-, 0]$, and a probability of resonance capture can be computed:

$$P_c \equiv \frac{\Delta_+ + \Delta_-}{\Delta_-}. \quad (11)$$

With the exception of Equation 9, the above outlines the argument given in [Henrard \(1982\)](#). Similar conclusions can be drawn for trajectories originating in zone I.

3.3 Zone II Initial Conditions

The fates of trajectories originating in zone II, which librate about the CS2, also depend on Δ_{\pm} . This implies $h_i > 0$. We identify the following possibilities:

- $\Delta_+ + \Delta_- > 0$: trajectories near the separatrix are driven back into zone II over the course of a full libration, therefore any trajectory originating in zone II is bound to zone II. Note that this alone need not imply convergence to CS2, e.g. for a non-dissipative system.
- $\Delta_+ + \Delta_- < 0, \Delta_+ > 0, \Delta_- < 0$: trajectories near the separatrix are driven back into zone II along C_+ but out of zone II along C_- , the net effect amounting to expulsion. Since expulsion cannot occur along C_+ , the only permitted transition is $\text{II} \rightarrow \text{III}$. Vice versa of course if the signs of Δ_{\pm} are swapped while still satisfying $\Delta_+ + \Delta_- < 0$.
- $\Delta_{\pm} < 0$: trajectories near the separatrix tend to be ejected along both C_{\pm} . Which zone the trajectory enters is then probabilistic: it enters zone I with probability $\frac{\Delta_+}{\Delta_+ + \Delta_-}$ and zone III with probability $\frac{\Delta_-}{\Delta_+ + \Delta_-}$.

It bears noting that in the non-dissipative limit, this result is equivalent to ([Henrard & Murigande 1987](#)), which computes these probabilities using change in enclosed phase space area.

3.4 Equivalence to Stable/Unstable Manifold Splitting

We now establish equivalence to an alternative formulation popular in dynamical systems that is more graphically intuitive. For simplicity, we will take $\dot{\eta} = 0$.

If we return to the unperturbed Hamiltonian system, recall that CS4 is joined to itself by an infinite-period orbit. For a given saddle point, we may define the *stable manifold* W_s of a saddle point to be the set of points whose forward evolution converges to the saddle point. Similarly, we may define the *unstable manifold* W_u of a saddle point to be the set of points that originated from the saddle point, or whose backwards evolution converges to the saddle point. A *saddle connection* is when the unstable manifold of one saddle point and the unstable manifold of another saddle point are degenerate. It is evident that the separatrix is formed of two saddle connections: C_+ is the unstable manifold of CS4 at $\phi = 2\pi$ and the stable manifold of CS4 at $\phi = 0$.

In the presence of a small perturbation, the stable and unstable manifolds generally separate, as the perturbations along the saddle connection will generally be different going forwards and backwards in time. The separation distance as a function of time along the

unperturbed trajectory can be computed via *Melnikov's Method*

$$d(t_0) = \frac{\epsilon}{|f(q^0(-t_0))|} \int_{-\infty}^{\infty} f(q^0(t - t_0)) \wedge g(q^0(t - t_0), t) dt. \quad (12)$$

The notation used here is that of [Guckenheimer & Holmes \(1983\)](#), where $d(t_0)$ is the distance between the stable/unstable manifolds at time t_0 along the heteroclinic orbit, $f = (\dot{\mu}^{(0)}, \dot{\phi}^{(0)})$, $\epsilon g = (\dot{\mu}^{(1)}, \dot{\phi}^{(1)})$ a general time-dependent perturbation, $q^0(t)$ is the unperturbed trajectory along the saddle connection (time coordinate defined such that $t = 0$ coincides with the “middle” of the infinite trajectory), and \wedge is the wedge product.

We will assume ϵg is not explicitly time-dependent, characteristic of secular/averaged equations in astrophysics, then the integral above is simply the familiar

$$d(t_0) \left| \vec{\nabla} H^{(0)} \right| (t_0) = \epsilon \int_{-\infty}^{\infty} \dot{\mu}^{(0)} \dot{\phi}^{(1)} - \dot{\phi}^{(0)} \dot{\mu}^{(1)} dt. \quad (13)$$

The right hand side is just the total change in $H^{(0)}$ over the saddle connection though, equivalent to our Equation 10 in the $\dot{\eta} = 0$ limit. The left hand side on the other hand is exactly $\left| \vec{d} \cdot \vec{\nabla} H^{(0)} \right|$ where the displacement is along $\vec{\nabla} H^{(0)}$. Thus, the effect of the Δ_{\pm} is to split the stable/unstable manifolds along the saddle connections.

Visually, this is depicted in [Figure 3](#). Note that: trajectories starting in zone III below W_s^R fail to separatrix cross; those between W_s^R and W_s^L continue between W_u^R and W_s^L , eventually escaping; those between W_s^L and W_u^L are securely captured, and no trajectories can begin above W_u^L at $\phi = 0$.

The saddle connection splitting is easiest to measure where $\vec{\nabla} H^{(0)} \propto \hat{\phi}$, where $\dot{\mu} = 0$, and Equation 13 reduces to just $\Delta\mu \frac{\partial H^{(0)}}{\partial \mu} = \Delta H^{(0)}$. Then the capture probability must be given by ratio of $\Delta\mu$ separating W_s^L, W_u^L to $\Delta\mu$ separating W_s^R, W_u^L . These $\Delta\mu$ values are those given in the title, and the resultant P_c capture probability is also quoted.

Finally, the connection between subsection 3.1 and subsection 3.4 is evident: the ratio of the $\Delta\mu$ values is simply

$$P_c = \frac{\Delta\mu(W_s^L, W_u^L)}{\Delta\mu(W_s^R, W_u^L)}, \quad (14)$$

$$= \frac{\Delta H_-^{(0)} + \Delta H_+^{(0)}}{\Delta H_-^{(0)}}. \quad (15)$$

This is exactly Equation 11 when $\dot{\eta} = 0$.

4 PROBLEM 1: ADIABATIC CAPTURE

Here we will adiabatically vary η . This problem is extensively covered in existing work e.g. ([Henrard & Murigande 1987](#)).

4.1 Spindown Model, $\dot{\eta} > 0$ (few sims)

We may first consider the unperturbed Hamiltonian system with $\frac{d\eta}{dt} = \frac{\eta}{t_{\eta}}$ growth with characteristic timescale t_{η} . Again rescaling time $\tau \equiv \alpha t$ and defining $\epsilon \equiv \frac{1}{\alpha t_{\eta}}$, we obtain

$$\frac{d\eta}{d\tau} = \epsilon\eta, \quad (16)$$

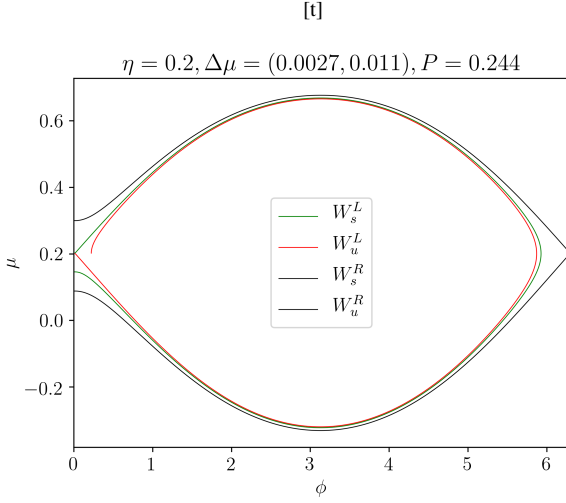


Figure 3. Sample plot of saddle connection breaking in the presence of weakly non-Hamiltonian dissipation. Equations are used from Section 5. Stable and unstable manifolds are indexed such that superscript L/R belongs to the saddle point at left/right. $\Delta\mu$ represent the manifold separations, resulting in capture probability P_c prediction per Equation 14. Numerical simulations predict $P_c \approx 0.252$.

where $\epsilon > 0$. Such a model is motivated e.g. when a planet's spin \hat{s} orbits a host star with angular momentum \hat{l} while the star spins down; $\dot{\alpha} < 0$ here, and $\eta' > 0$.

We then seek Δ_{\pm} , determined by

$$\begin{aligned} \Delta_{\pm} &= \int_{C_{\pm}} \frac{\partial h}{\partial \eta} \eta' d\tau, \\ &= \int_{C_{\pm}} \frac{\partial h}{\partial \eta} \eta' d\phi. \end{aligned} \quad (17)$$

We must proceed carefully since $\phi' \rightarrow 0$ at the endpoints of C_{\pm} ; careful work shows these zeros cancel against zeros of $\frac{\partial h}{\partial \eta}$, and

$$\Delta_{\pm} = \int_{C_{\pm}} \eta' \left(\cos I \mp \sin I \sqrt{\frac{1 - \cos \phi}{2\eta \sin I}} \right) d\phi, \quad (18)$$

$$= \mp 2\pi\epsilon\eta \cos I + 4\epsilon\sqrt{\eta \sin I}. \quad (19)$$

Call η_{\star} the value of η at which a trajectory encounters the separatrix. There are then three possibilities:

- For $\eta_{\star} < \frac{4 \sin I}{\pi^2 \cos^2 I}$, we obtain $\Delta_{\pm} > 0$. In this regime, all separatrix encounters originating in zones I/III result in secure capture (see subsection 3.2), while all trajectories originating in zone II do not experience separatrix encounter. For $I = 20^\circ$, this condition equates to $\eta_{\star} \lesssim 0.16$. This condition is not to be taken too exactly, as all our calculations are performed in the small η limit. Select simulations in $\eta_{\star} \lesssim 0.1$ are in agreement with the secure capture prediction. An example of such a simulation is presented in Figure 4.

- If $\eta_{\star} > \frac{4 \sin I}{\pi^2 \cos^2 I}$, $\eta_{\star} < \eta_c$, then the separatrix still exists, and $\Delta_+ < 0, \Delta_- > 0$. This implies: zone I + zone II trajectories do not experience separatrix encounters, while zone III trajectories are captured into zone II with probability

$$P_c = \frac{8\sqrt{\eta_{\star} \sin I}}{2\pi\eta_{\star} \cos I + 4\sqrt{\eta_{\star} \sin I}}. \quad (20)$$

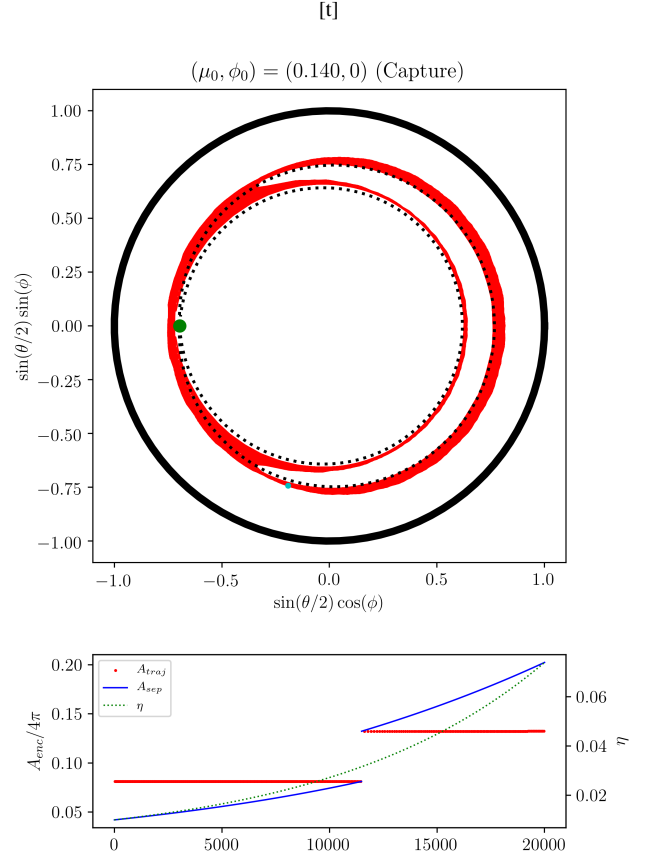


Figure 4. Simulation with initial condition in zone I subject to $\eta' = \epsilon\eta$, where $\epsilon = 10^{-4}$. The top panel shows the trajectory (red) starting with initial condition $\mu_0 = 0.140, \phi_0 = 0$ (green dot) and separatrix at separatrix crossing (dashed black) in the labelled coordinates. The end of the simulation is labelled in the blue cyan dot. The bottom panel shows the evolution of the enclosed area by the trajectory (red dots), area of the separatrix (blue) and η (dotted green) over time.

- Further evolution from either of the above two cases, as well as the case where no separatrix encounter occurs before $\eta > \eta_c$, is governed simply by conservation of adiabatic invariant/action variable

$$I \equiv \oint \cos \theta d\phi. \quad (21)$$

4.2 Spinup Model, $\dot{\eta} < 0$ (no sims)

If instead $\epsilon < 0$, then the separatrix area shrinks over time. For initial values $\eta > \eta_c$, the separatrix appears over time and the scenario is analyzed in (Anderson & Lai 2018).

If η decreases past critical value $\frac{4 \sin I}{\pi^2 \cos^2 I}$, i.e. $\Delta_{\pm} < 0$, then the separatrix appears. Here, trajectories in zones I/III do not experience separatrix encounter while trajectories in zone II transition into zones I/III with probabilities given respectively (see subsection 3.3):

$$\begin{aligned} P_{II \rightarrow I} &= \frac{2\pi\eta_{\star} \cos I + 4\sqrt{\eta_{\star} \sin I}}{8\sqrt{\eta_{\star} \sin I}}, \\ P_{II \rightarrow III} &= \frac{-2\pi\eta_{\star} \cos I + 4\sqrt{\eta_{\star} \sin I}}{8\sqrt{\eta_{\star} \sin I}}. \end{aligned} \quad (22)$$

4.3 Nontrivial Test Problem, “Problem 1.5” (sims)

It is clear that η' in Equation 18 being the same sign along both C_{\pm} is the source of guaranteed capture during spindown. In order to test that Equation 11 is not only qualitatively correct but also quantitatively exact, we seek to simulate a problem with probabilistic behavior. **Note: This section is probably superseded by subsection 4.2 or Section 6..** We investigate test problem where η is varied following

$$\eta' = \epsilon \eta \mu. \quad (23)$$

This is a pure mathematical exercise, but resembles weak tidal friction in the subsynchronous rotation regime.

Straightforward evaluation of Equation 18 yields

$$\Delta_{\pm} = \pm \epsilon \eta_{\star} \left[2\pi \sin I \pm 12\sqrt{\eta_{\star}} \sin I \cos I + 2\pi \eta_{\star} \cos^2 I \right]. \quad (24)$$

It bears noting that we must evaluate these integrals at $\eta = \eta_{\star}$ the value at separatrix crossing. Since η evolves over time, η_{\star} depends on initial conditions. While one might expect the adiabatic invariance of the action variable determines η_{\star} , this turns out to be slightly inaccurate for reasons (I haven’t worked this out convincingly yet).

Since $|\Delta_+| > |\Delta_-|$, separatrix encounters originating in zone III always result in capture. However, encounters originating in zone I experience capture probability

$$P_c(\eta_{\star}) = \frac{24 \cos I \sqrt{\eta_{\star}} \sin I}{2\pi \sin I + 12\sqrt{\eta_{\star}} \sin I \cos I + 2\pi \eta_{\star} \cos^2 I}. \quad (25)$$

To test this capture probability, we test capture probability at a variety of I for similar ICs. For fixed initial condition (μ_0, ϕ_0) in zone I, we vary the initial $\eta \in [0.01, 0.02]$ and $\epsilon \in 10^{-3, -2}$. In this way, every simulation experiences probabilistic separatrix crossing at roughly comparable times. We then repeated this procedure for three different values $I = 10^\circ, 20^\circ, 25^\circ$. A natural spread in η_{\star} was observed at each I value, which permitted comparison to Equation 25 independently. The results for the three I values are presented in Figure 5, where good agreement with Equation 25 is shown.

5 PROBLEM 2: WEAKLY DISSIPATIVE HAMILTONIAN

5.1 $\eta < \eta_c$, Separatrix Encounters (sims)

We next consider a toy separatrix crossing problem in the $\eta = 0$ limit, the case discussed in subsection 3.4. Consider adding to the Hamiltonian Cassini State problem an additional aligning term $\left(\frac{d\theta}{dt}\right)^{(1)} = -\frac{1}{t_s} \sin \theta$ that favors alignment $\theta = 0$ on synchronization timescale t_s . This translates to equation of motion

$$\frac{d\hat{s}}{d\tau} = \left(\hat{s} \cdot \hat{l}\right) \left(\hat{s} \times \hat{l}\right) - \eta \left(\hat{s} \times \hat{l}_p\right) - \epsilon \sin \theta \hat{\theta}. \quad (26)$$

We have divided Equation 4 by α and defined $\tau \equiv \alpha t$, $\epsilon \equiv \frac{1}{\alpha t_s}$. The equations of motion for canonical variables $\mu \equiv \cos \theta$, ϕ are

$$\phi' = -\cos \theta + \eta \left(\cos I + \sin I \frac{\mu}{\sqrt{1-\mu^2}} \cos \phi \right), \quad (27a)$$

$$\mu' = -\eta \sin I \sin \theta \sin \phi \left[+\epsilon \left(1 - \mu^2 \right) \right]. \quad (27b)$$

Primes denote $\frac{d}{d\tau}$. The bracketed term in μ' is the perturbation component. We will take $\alpha, \epsilon > 0$, which will result in separatrix encounters originating in zone III, but an identical procedure for $\epsilon < 0$ describes separatrix encounters originating in zone I.

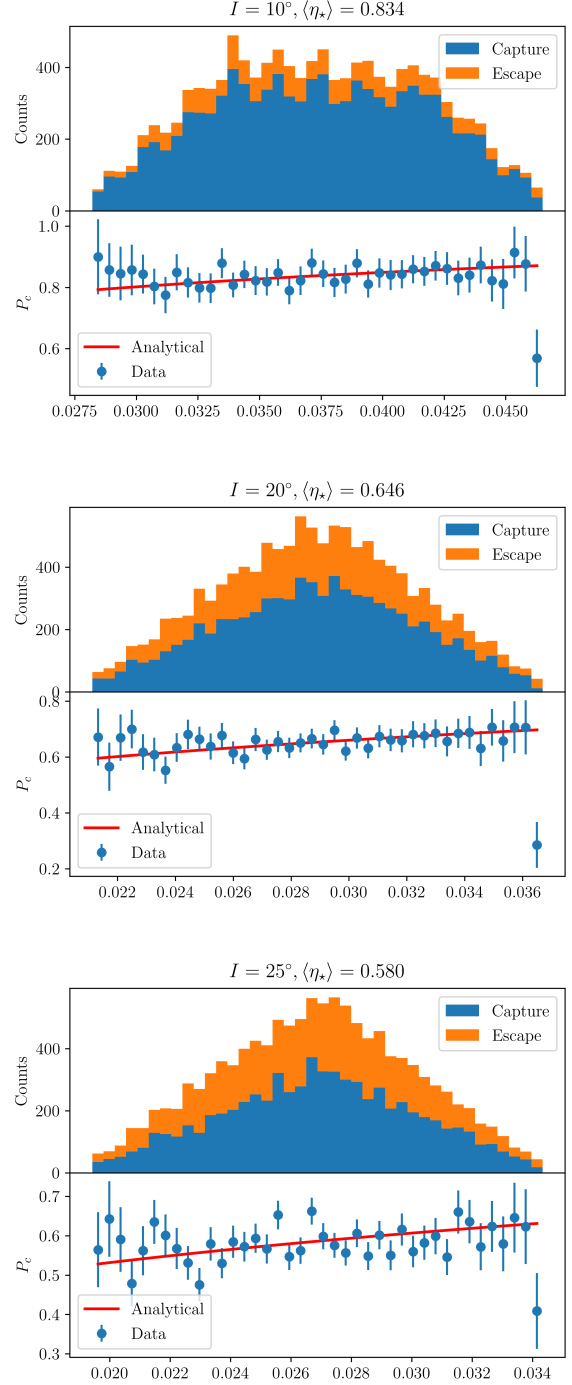


Figure 5. Simulations depicting $P_c(\eta_{\star})$ at three different values $I = 10^\circ, 20^\circ, 25^\circ$ compared to analytical estimate Equation 25. The top panel is a stacked histogram showing the capture (into separatrix) and escape occurrence counts at each η_{\star} . The bottom panel are the inferred estimates of $P_c(\eta_{\star})$ (capture probability) in blue and analytical curve in red. Uncertainties in $P_c(\eta_{\star})$ from data are estimated as \sqrt{N} where N is the number of captures per bin. Also reported is the average value of η_{\star} .

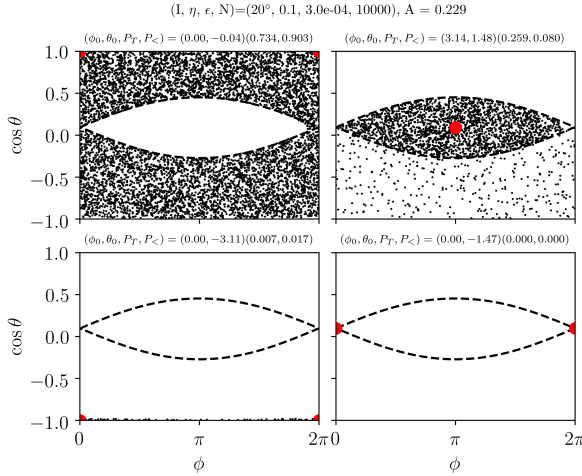


Figure 6. Plot of the CSs that initial conditions converge to. Each subplot has a set of initial conditions (black dots) and the CS (red dot) that each of these initial conditions converge to. Initial conditions are chosen uniformly in (μ, ϕ) coordinates. Key features to note are secure convergence to CS1 for all zone I initial conditions, probabilistic convergence to CS1 or CS2 for zone III initial conditions (first half of subsection 5.1), and secure convergence to CS2 for all zone II initial conditions (second half of subsection 5.1). The parameters for the simulation are in the title.

With a dissipative term that favors alignment, we expect that separatrix encounters can only occur from zone II and zone III. We will focus on the outcomes of trajectories originating in zone III for now. We now aim to compute Equation 11, for which we need:

$$\Delta_{\pm} = \int_{C_{\pm}} \phi' \epsilon (1 - \mu^2) dt, \\ = \mp 2\pi \left(1 - 2\eta \sin I - \eta^2 \cos^2 I \right) + 16 \cos I \eta^{3/2} \sqrt{\sin I}. \quad (28)$$

Note that along C_{\pm} that $d\phi$ has sign \mp respectively. From these two integrals, we obtain

$$P_c = \frac{16\eta^{3/2} \cos I \sqrt{\sin I}}{\pi (1 - 2\eta \sin I - \eta^2 \cos^2 I) + 8\eta^{3/2} \cos I \sqrt{\sin I}}. \quad (29)$$

As evidence, we provide the following table of separatrix capture probabilities in Table 1.

It may be noted that the numerical P_c are systematically low compared to their analytical estimates. This has a clean explanation: initial conditions that start too close to the separatrix violate the assumption where h_i is uniformly distributed on $[-\Delta_-, 0]$. In particular, most of the points near the separatrix and in zone III are escaping points, as can be visually seen in Figure 3. A systematic underdensity of points converging to CS2 (separatrix capture) can be seen on the right hand side of the plot near the separatrix in Figure 6.

A further interesting feature in Figure 6 is a small portion of points in zone II near CS4 at $\phi = 2\pi$ that escape. These points accrue Δ_+ on their first orbit and escape without librating. Visually, this zone is obvious in Figure 3 as the separation between $W_s^{(1)} \cup W_u^{(1)}$ and $W_s^{(0)} \cup W_u^{(0)}$ near $\phi = 2\pi$.

For trajectories originating in zone II, numerical simulations indicate they can never leave the separatrix. This can be understood quantitatively (excepting the few initial conditions in Figure 6 discussed above). For any orbit in zone II that completes a full libration

over contour C , the total change in h is given

$$\Delta h = \epsilon \oint_C (1 - \mu^2) d\phi. \quad (30)$$

Since C is a closed contour, any terms that are symmetric on the top and bottom legs of C vanish. If we decompose $\mu(\phi) \equiv \bar{\mu} \pm \mu'(\phi)$ where $\bar{\mu}$ is the average value of $\mu(\phi)$ over C and $\mu'(\phi) \geq 0$ everywhere, then it is clear

$$\Delta h = 2\epsilon \int_0^{2\pi} 2\bar{\mu} \mu'(\phi) d\phi. \quad (31)$$

Now, since $\mu'(\phi) \geq 0$ everywhere, and $\bar{\mu} \in [\mu_2, \mu_4] > 0$ as well, $\Delta h \geq 0$ necessarily, equality only exactly at CS2. And so, *all full librations in zone II will be driven towards CS2* (the point of maximum h and $H^{(0)}$).

5.2 $\eta > \eta_c$, Convergence to CS2 (no sims)

While not strictly within the purview of this paper, we can also prove that once $\eta > \eta_c$ and the separatrix vanishes, all trajectories converge to CS2. This follows naturally by considering the change $\Delta H^{(0)}$ over any orbit

$$\Delta H^{(0)} = \oint \epsilon (1 - \mu^2) d\phi. \quad (32)$$

Visual inspection of Figure 1 shows that all orbits either circulate $\phi' > 0$ or librate counterclockwise very near CS2. For any circulating $\phi' > 0$ orbit, $\Delta H^{(0)} > 0$ is enforced. For any counterclockwise libration near CS2, the same argument as the zone II initial conditions from subsection 5.1 above apply, where $\Delta H^{(0)} \geq 0$ with equality only at CS2 itself.

6 PROBLEM 3: COMBINED PERTURBATIONS (SIMS)

We now consider the combined problem, where the EOMs for Problem 2 (Equation 27) are used in conjunction with the simplest $\eta' = \delta\eta$, the same as Equation 16. Evaluation of Δh along C_{\pm} is simply combining the results of Equation 19 and Equation 28. The result is

$$\Delta_{\pm} = \epsilon \left[\mp 2\pi \left(1 - 2\eta \sin I - \eta^2 \cos^2 I \right) + 16 \cos I \eta^{3/2} \sqrt{\sin I} \right] \\ + \delta \left[\mp 2\pi \eta \cos I + 4\sqrt{\eta \sin I} \right]. \quad (33)$$

Thus, the capture probability from a zone III initial condition into the separatrix is

$$P_c \approx \frac{(32\eta_{\star} \cos I + 8f) \sqrt{\eta_{\star} \sin I}}{2\pi (1 - 2\eta_{\star} \sin I + f\eta_{\star} \cos I) + (16\eta_{\star} \cos I + 4f) \sqrt{\eta_{\star} \sin I}}. \quad (34)$$

An η_{\star}^2 term has been dropped from the denominator, and $f \equiv \frac{\delta}{\epsilon}$ measures the relative strength of the two perturbations. Note that $f = 0$ reduces to Section 5.

The accuracy of Equation 34 is illustrated in Figure 7. A small deviation can be noticed at larger η_{\star} values as f is increased. This is attributed to the separatrix becoming significantly asymmetric around $\eta \sim 0.15$, therefore our Equation 6 is no longer an accurate approximation. When $f = 0$, the small deviations are significantly suppressed as the numerator scales with $\eta_{\star}^{3/2}$ compared to when $f \sim 1$, where the numerator instead scales with $\eta_{\star}^{1/2}$.

η	0.025	0.05	0.1	0.2
Numerical P_c	0.010 ± 0.002	0.029 ± 0.003	0.082 ± 0.004	0.256 ± 0.006
Analytical P_c	0.0112	0.0320	0.0915	0.2627.

Table 1. Capture probability for four different values of η , all using $\epsilon = 3 \times 10^{-4}$. Different values of ϵ were tried $\epsilon \in 10^{[-2, -4]}$ with no effect on P_c . 10000 random initial conditions uniformly distributed in (μ, ϕ) were used for the numerical calculations, of which roughly 1/2 experience separatrix crossing. Numerical uncertainties are estimated as \sqrt{N} where N is the count per bin.

7 PROBLEM 4: WEAK TIDAL DISSIPATION (SIMS)

7.1 Solution

We consider now the full Cassini State system with under weak tidal friction (see e.g. Lai (2012)). Note that generally $|g|$ is a constant under weak tidal friction, as it is an orbit-orbit coupling term, while $\alpha \propto s$. Defining then s_c critical spin such that $\frac{s}{s_c} \equiv \frac{\alpha}{|g|} 1$ and Ω_1 the spin that \hat{s} is coupled to, we can write down fully coupled evolution equations for (μ, ϕ, s) :

$$\frac{d\phi}{d\tau} = \frac{s}{s_c} \mu - \left(\cos I + \sin I \frac{\mu}{\sqrt{1-\mu^2}} \cos \phi \right), \quad (35a)$$

$$\frac{d\mu}{d\tau} = -\sin I \sin \phi + \epsilon \left(1 - \mu^2 \right) \left(\frac{2\Omega_1}{s} - \mu \right), \quad (35b)$$

$$\frac{ds}{d\tau} = \epsilon 2\Omega_1 \left(\mu - \frac{s}{2\Omega_1} (1 + \mu^2) \right). \quad (35c)$$

The expressions for $H^{(0)}, H_{sep}$ can also be written down

$$H(\mu, \phi; s) = -\frac{s}{s_c} \frac{\mu^2}{2} + \mu \cos I - \sin I \sqrt{1 - \mu^2} \cos \phi. \quad (36)$$

$$H_{sep}(s) = -\sin I + \frac{s_c}{2s} \cos^2 I. \quad (37)$$

Note that here s takes the role of adiabatically-varying parameter. Thus, when computing Δ_{\pm} along the separatrix using Equation 10, there are two contributions. In particular, we write

$$\Delta_{\pm} = \int_{C_{\pm}} \dot{\mu}^{(1)} + \frac{\dot{s}}{\dot{\phi}^{(0)}} \frac{\partial h}{\partial s} d\phi. \quad (38)$$

Both of these integrals were performed in preceeding sections, and we may express in closed form (dropping some terms for simplicity)

$$\Delta_{\pm} \approx \epsilon \left\{ \mp \frac{4\pi\Omega_1}{s} + 8\sqrt{\frac{s_c}{s}} \sin I \right\} + \epsilon \left\{ \frac{\Omega_1 s_c}{s^2} \left[\pm 8\sqrt{\frac{s_c}{s}} \sin I \left(\frac{s}{2\Omega_1} - \frac{s_c \cos I}{s} \right) + 4\pi \frac{s_c}{s} \sin I \right] \right\}. \quad (39)$$

We can then compute separatrix capture probability from zone III (which is $P_c = \frac{\Delta_+ + \Delta_-}{\Delta_-}$), again evaluating at $s = s_{\star}$:

$$P_c(s_{\star}) = \frac{16\sqrt{\frac{s_c}{s_{\star}}} \sin I + 8\pi \frac{s_c}{s_{\star}} \sin I}{\frac{4\pi\Omega_1}{s_{\star}} - \frac{8\Omega_1 s_c}{s_{\star}^2} \sqrt{\frac{s_c}{s_{\star}}} \sin I \left(\frac{s_{\star}}{2\Omega_1} - \frac{s_c \cos I}{s_{\star}} \right)}. \quad (40)$$

Note that for $\frac{s_c}{s_{\star}} < \eta_c$ that no separatrix (or resonance) exists anymore, so we will generally assume $s_{\star} \gtrsim s_c, \Omega_1$.

To test Equation 40, we generate an evenly spaced grid of initial conditions (μ_0, ϕ_0) and initialize $s_0 = 10$. We then record s_{\star} and the final outcome of the trajectory over many simulations. The agreement of Equation 40 with data can be observed in Figure 8.

7.2 Estimating s_{\star}

In Section 4, the capture probability $P_c(\eta_{\star})$ depended on η_{\star} which could be determined by conservation of the action variable I . Such an argument is not possible in the weak tidal prescription as the system is dissipative thanks to $\dot{\mu}^{(1)}$ (see Equation 35).

However, instead we can write down $\frac{dh}{d\tau}$, just as Equation 9. Since the initial value of h can be computed from initial conditions, the ODE can simply be integrated numerically to find τ_{\star} the separatrix crossing time. In fact, for μ far from the separatrix, $\frac{dh}{d\tau} \approx \frac{3s\mu^2}{2s_c}$, predicting

$$\tau_{\star} = \frac{h(t=0)}{3s\mu^2/2s_c} + C, \quad (41)$$

where C depends on the details of $\frac{dh}{d\tau}$ near the separatrix. This is in good agreement with measurement (see top panel of Figure 9).

7.3 High Misalignment as an Attractor

Careful examination of Equation 39 reveals that for sufficiently large s_c , Δ_+ changes sign and becomes positive. When $\Delta_+ < 0$, trajectories in zone I above the separatrix cannot enter the separatrix, as h decreases over an orbit. However, if $\Delta_+ > 0$, then trajectories in zone I can also enter the separatrix. The critical value of s_c where Δ_+ changes sign as a function of s can thus be determined analytically. TODO write down the formula and check it against my numerical solution earlier.

Furthermore, $\frac{d\mu}{d\tau} < 0$ for $\mu > \frac{2\Omega_1}{s}$, it is clear that if s is initially large, then aligned states $\mu > 0$ are driven towards misalignment and the separatrix, where they may then be captured for sufficiently large s_c . We find that $s_c \gtrsim 0.5\Omega_1$ is sufficient that an initial spin of $s_0 = 10$ will *always* be captured into CS2.

TODO Maybe this is worth a real plot?

REFERENCES

- Anderson K. R., Lai D., 2018, Monthly Notices of the Royal Astronomical Society, 480, 1402
 Guckenheimer J., Holmes P. J., 1983, Nonlinear oscillations, dynamical systems, and bifurcations of vector fields. Springer-Verlag, New York
 Henrard J., 1982, Celestial Mechanics and Dynamical Astronomy, 27, 3
 Henrard J., Murigande C., 1987, Celestial Mechanics, 40, 345
 Lai D., 2012, Monthly Notices of the Royal Astronomical Society, 423, 486

¹ s_c has interpretation *critical spin* such that $\alpha, |g|$ are equal.

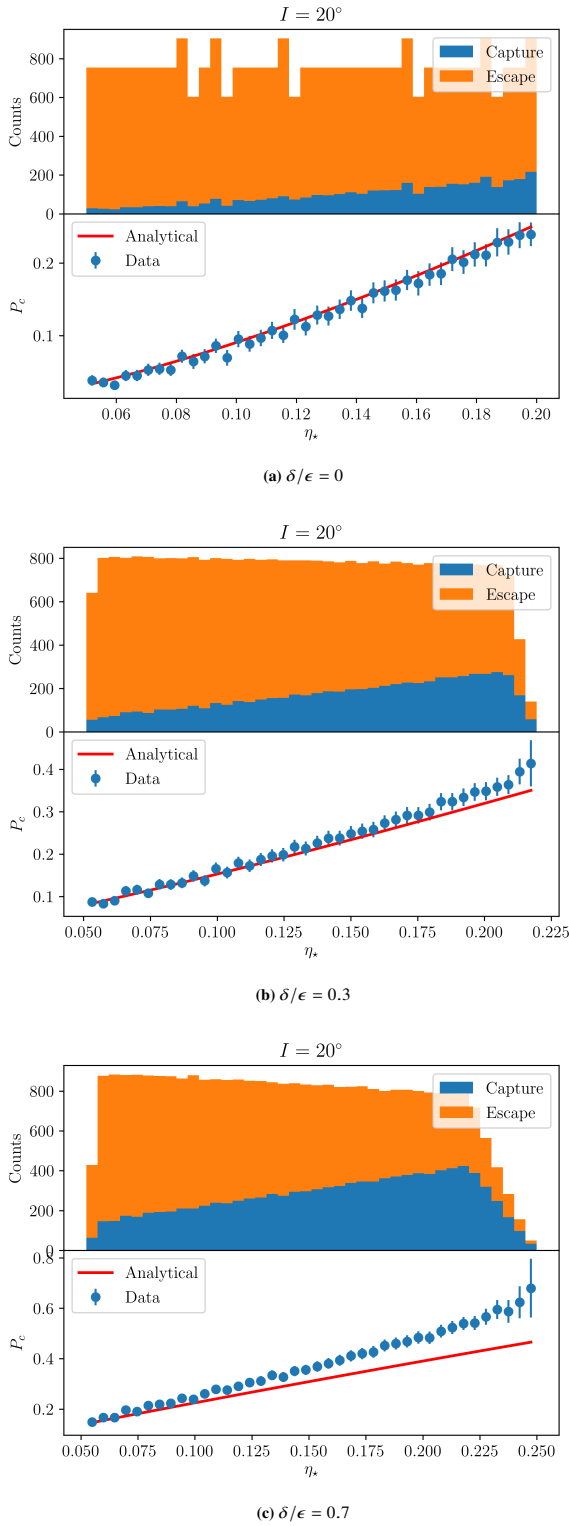


Figure 7. Histogram of simulation and inferred $P_c(s_*)$ compared with Equation 34, where $f = \delta/\epsilon$ is varied. 3×10^4 initial conditions were used for both plots. While the $f = 0$ case indicates perfect agreement, the other two cases show increasingly large deviations at larger s_* .

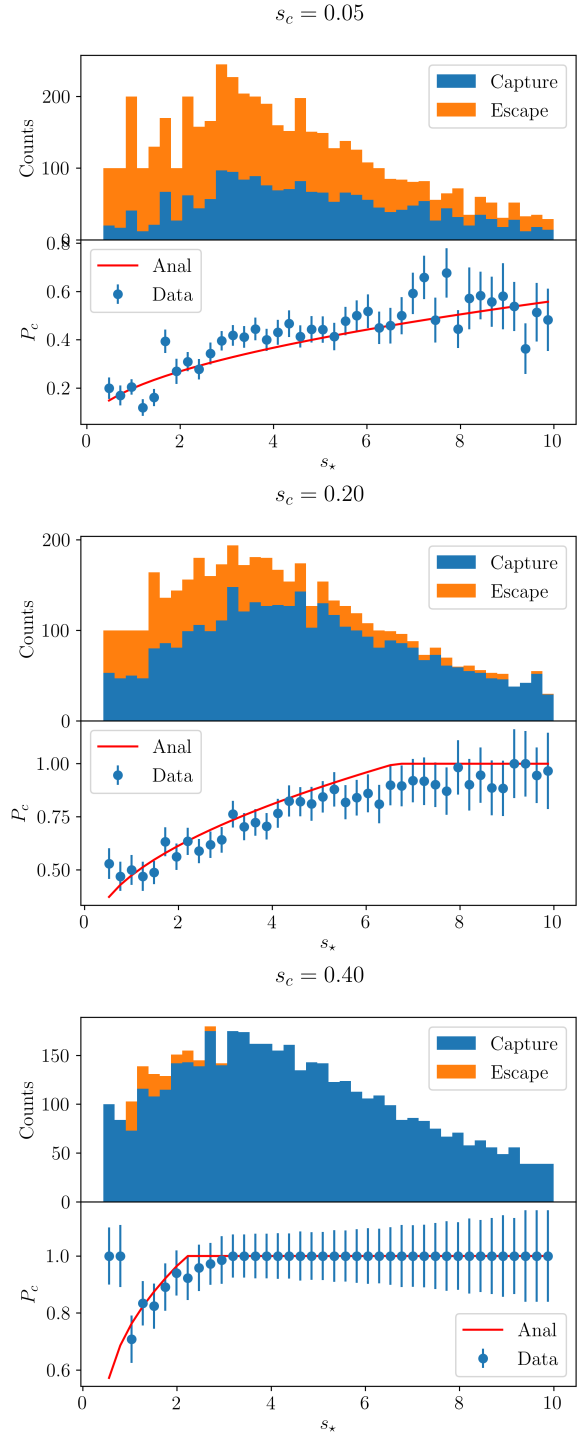


Figure 8. Histogram of simulation and inferred $P_c(s_*)$ compared with Equation 40. s_c used are numbered at the top of each plot. 10^4 simulations were used for each plot, and a single $I = 20^\circ$ was used.

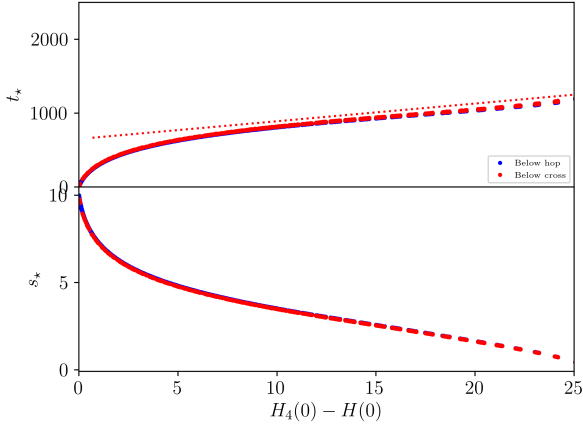


Figure 9. TODO make this plot actually look reasonable. The top and bottom panels show t_* , s_* as a function of $-h = H_{sep} - H$. The dotted red line in the top panel is $t_* = \frac{h}{3s\mu^2/2s_c} + C$ where C is a fitting parameter determined by the behavior of $\frac{dh}{d\tau}$ near the separatrix. This demonstrates that the separatrix arrival time is well-described by [Equation 41](#).